Available online at www.sciencedirect.com
ScienceDirect
Computer Coupling of Phase Diagrams and Thermochemistry 31 (2007) 330–342
www.elsevier.com/locate/calphad

Thermodynamic description of the Ti–O system using the associate model for the liquid phase

M. Cancarevic*[,1], M. Zinkevich, F. Aldinger

Max-Planck Institut für Metallforschung und Institut für Nichtmetallische Anorganische Materialien der Universität Stuttgart, Heisenbergstr. 3, D-70569 Stuttgart, Germany

Received 17 October 2006; received in revised form 12 January 2007; accepted 28 January 2007
Available online 6 March 2007

Abstract

The thermodynamic assessment of the Ti–O system was carried out by the CALPHAD method using the associate model for the liquid phase and the compound energy formalism for the solid phases. The derived set of parameters gives reasonable representation of the phase equilibria and thermodynamic properties of phases in the Ti–O system, while providing good extrapolation capability.

Keywords: Titanium; Oxygen; Phase diagram; Thermodynamics; Associate model

1. Introduction

Understanding of phase equilibria and thermodynamic properties in the Ti–O system is of basic interest for manufacturing and controlling the properties of Ti and its alloys, metallurgical slags, and oxide ceramic materials containing titanium. A review of the literature data on the Ti–O system, which includes publications before 1987, has been presented by Murray and Wriedt [1]. There are a few modifications of the experimental Ti–O phase diagram [2–5] which differ markedly from each other except for the *bcc*/*hcp* phase boundaries and the wide stability range of the *fcc* monoxide (TiO_x).

The first modeling of the Ti–O system was done by Kaufmann and Clougherty [6], including the thermodynamics description of *bcc*, *hcp*, and TiO_x solid solutions. Saunders and Chandrasekaran [7], Pajunen and Kivilahti [8], and Lee [9,10] published thermodynamic assessments of Ti–O system covering the composition range from pure Ti up to TiO_2, where the different models for TiO_x solid solution as well as for the liquid phase were applied. Magneli phases and the non-stoichiometry of rutile were first taken into account in the work of Eriksson and Pelton [11], for the modeling of the Ti_2O_3–TiO_2 subsystem. Their dataset was recently modified by Kang et al. [12] in order to remove a metastable liquid miscibility gap near Ti_2O_3. The most extensive evaluation of the Ti–O system was done by Waldner and Eriksson [13]. They presented a complete Ti–O phase diagram from pure titanium to gaseous oxygen including Magneli phases. For the modeling of the TiO_x solid solution, the two-sublattice definition based on the bond energy model [14,15] was adopted.

As for the liquid phase, the simple substitutional model with the non-ideal mixing between liquid titanium and liquid oxygen was used in Refs. [6–8], while the two-sublattice ionic liquid model was employed in Refs. [9,10,13] and the quasichemical model was adopted in Refs. [11,12]. A substitutional model is clearly a very crude approach for a system with strong interactions, such as Ti–O. The two-sublattice ionic liquid model is physically well-sounded; however, it may result in unexpected miscibility gaps in higher-order systems at high temperatures. For instance, in the ternary Cu–Ti–O system, the description of ionic liquid is $(Cu^{1+}, Cu^{2+}, Ti^{2+}, Ti^{3+}, Ti^{4+})_p(O^{2-}, Va^{q-})_q$. The calculated tie-lines at 1500, 2200 and 2400 K [16] show, however, that a Ti-rich oxide liquid coexists with a Cu-rich metallic liquid, giving rise to the extended miscibility gap. Despite the fact

* Corresponding address: Max-Planck Institute for Metal Research, Heisenbergstr. 3, D-70569 Stuttgart, Germany. Tel.: +49 711 6893 107; fax: +49 711 6893 131.
E-mail address: cancar@mf.mpg.de (M. Cancarevic).
[1] Permanent address: Institute of Nuclear Science "Vinca", Department of Material Science, Post Box 522, 11000 Belgrade, Serbia.

0364-5916/$ - see front matter © 2007 Elsevier Ltd. All rights reserved.
doi:10.1016/j.calphad.2007.01.009

Table 1
Selection of experimental information for the Ti–O system: phase diagram data

Ref.	Experimental technique	Measured quantity, temperatures, compositions
[2]	X-ray diffraction, metallographic analysis, optical pyrometry	Phase equilibria in the Ti–O system between 973 and 2173 K, up to 56 at.% O, solubility of oxygen in *bcc*, *hcp* and TiO_x phases (phase boundaries), invariant reactions and liquidus.
[3]	Microstructure analysis, vacuum fusion, absorptiometric method, optical pyrometry	Phase equilibria in the Ti–O system between 1023 and 2173 K, up to 60 at.% O, solubility of oxygen in *bcc*, *hcp* and TiO_x phases (phase boundaries), invariant reactions and liquidus.
[4]	X-ray diffraction, chemical analysis	Phase equilibria in the Ti–O system between 1173 and 1373 K over the composition range 0.33–0.56 at.% O (*hcp*/TiO_x, TiO_x/α-TiO, and TiO_x/Ti_2O_3 phase boundaries).
[20]	X-ray diffraction, metallographic analysis, microhardness test	Phase equilibria in the Ti–O system between 673 and 1073 K, up to 35 at.% O, solubility of oxygen in *hcp* phase (phase boundaries), ordered structure in the low temperature α-phase region based on the compositions Ti_6O and Ti_3O.
[21]	Analysis of diffusion specimens	Solubility of oxygen in *bcc* phase in the temperature range 1223-1687 K (*bcc*/*hcp* phase boundary).
[22]	Metallographic analysis, hardness test	Phase equilibria in the Ti–O system between 1123 and 1323 K, up to 3 at.% O (*bcc*/*hcp* phase boundary).
[23]	Thermoelectric power measurements, metallographic and chemical analysis	Solubility of oxygen in *bcc* and *hcp* phases between 1073 and 1423 K, up to 5 at.% O (*bcc*/*hcp* phase boundary).
[24]	X-ray diffraction, metallographic analysis, melting temperature measurements	Liquidus of the oxygen-rich part of the Ti–O system.
[25]	No information	Liquidus of the Ti_2O_3–TiO_2 subsystem.
[26]	X-ray diffraction, electron and optical metallography	Phase equilibria in the Ti–O system between 873 and 2013 K over the composition range 15–56 at.% O, solubility of oxygen in *hcp* phase (phase boundaries), ordered structure in the low-temperature α-phase region based on the compositions Ti_2O and Ti_3O as well as in the TiO_x region.
[27]	X-ray diffraction	Solubility of oxygen in TiO_x phase at 1573 K (*hcp*/TiO_x and TiO_x/Ti_2O_3 phase boundaries).
[28]	X-ray diffraction	Solubility of oxygen in *hcp* phase at 1273 K (*hcp*/TiO_x phase boundary).

Only data which were used in the present assessment are given.

that corresponding experimental data are missing, a very low solubility of copper in the Ti-rich oxide liquid as well as a very low combined solubility of titanium and oxygen in the Cu-rich liquid at high temperatures is unreasonable. The problem cannot be solved by including ternary interaction parameters. The appearance of such a liquid miscibility gap is affected by reciprocal reaction between species, which increases the Gibbs energy of liquid phase, and although the Gibbs energy of mixing can be negative over the whole composition range, inflection points give rise to the decomposition into two liquids. The sublattice model fails to describe the short-range ordering in the liquid and therefore it predicts a very strong tendency for demixing. Another deficiency of the ionic liquid model is the need to balance several contributions into the Gibbs energy of a liquid metal (e.g., Ti^{2+} : Va^{2-}, Ti^{3+} : Va^{3-}, Ti^{4+} : Va^{4-}), which causes additional complications. In contrast to the ionic two-sublattice model, the associate model (Cu, Cu_2O, O, Ti, TiO, $TiO_{1.5}$, TiO_2) describes summarily short-range ordered volume parts as associates and does not give rise to the liquid miscibility gap at 2200 and 2400 K, while the narrow miscibility gap originating from the Cu–O system exists on the calculated isothermal sections at 1500, 1550 and 1600 K [16]. Unfortunately, there is no direct translation of the ionic liquid model into the associate model. The quasichemical model for the liquid phase [11,12] may be superior to both ionic and associate formalisms in the range between oxide end-members from TiO to TiO_2 but, unfortunately, it cannot be applied for the description of metal-rich liquid.

The aim of the present work is to obtain a self-consistent thermodynamic description of the Ti–O system by means of the CALPHAD method [17,18], using an associate model for the liquid, which can successfully be used for calculations in multicomponent systems containing Ti and O, as well as the remodeling of the TiO_x solid solution using a compound energy formalism, which is compatible with most of the commercial software packages for thermodynamic calculations. It should be stressed that the objective is not to produce a new improved assessment of the Ti–O system compared to the previous works but rather to get a simplified description of the liquid phase. All computations were done using the Thermo-Calc software package [19].

2. Survey of literature information

The experimental database for the Ti–O system includes numerous investigations of phase equilibria and thermodynamic properties. Almost all these data have already been reviewed [1, 13] and only a summary is given here (Tables 1 and 2). The melting points of Ti_2O_3, Ti_3O_5, and TiO_2 assessed by Murray and Wriedt [1] are accepted in the present work. Both Ti_2O_3 and rutile melt congruently, while incongruent melting was reported for Ti_3O_5. A peculiarity of the Ti–O system is the existence of so-called Magneli phases, Ti_nO_{2n-1} ($n \geq 2$), which

Table 2
Selection of experimental information for the Ti–O system: thermodynamic data

Ref.	Experimental technique	Measured quantity, temperatures, compositions
[29]	EMF measurements	Chemical potential of oxygen in the temperature range 1000–1700 K over compositions $0.5 \leq O/Ti \leq 2.0$ (TiO_x, Magneli phases, rutile).
[30]	EMF measurements	Chemical potential of oxygen in the two-phase region of non-stoichiometric rutile and highest Magneli phase between 1123 and 1323 K.
[31]	EMF measurements, thermogravimetry, H_2/H_2O gas equilibration	Partial pressure of oxygen in the temperature range 1573–1873 K over the composition range $1.67 \leq O/Ti \leq 2.0$.
[32]	EMF measurements	Partial pressure of oxygen over the non-stoichiometric TiO_x solid solution and the two adjacent two-phase regions at 1323 K.
[33]	EMF measurements	Chemical potential of oxygen within the stability range of titanium dioxide between 1073 and 1273 K.
[34]	EMF measurements	Partial pressure of oxygen over the *bcc* solid solution (0.1–0.6 at.% O) between 1273 and 1423 K.
[35]	EMF measurements	Chemical potential of oxygen in the two-phase region, $Ti_2O_3 + Ti_3O_5$ from 1022 to 1495 K.
[36]	EMF measurements	Relative partial Gibbs energy of oxygen in the Ti_2O_3–Ti_3O_5 region at 1200 K.
[37]	EMF measurements	Partial molar Gibbs energy of oxygen of non-stoichiometric rutile at 1273 and 1373 K.
[38]	EMF measurements	Partial molar Gibbs energy of oxygen over the Magneli phases Ti_nO_{2n-1} for $4 \leq n \leq 10$ in the temperature range 1150–1273 K.
[39]	EMF measurements	Partial pressure of oxygen over the non-stoichiometric rutile at 1123 K.
[40]	EMF measurements, CO/CO_2 gas equilibration, thermogravimetry	Partial molar Gibbs energy of oxygen solution in TiO_{2-x} as a function of x between 982 and 1473 K
[41]	EMF measurements, thermogravimetry	Chemical potential of oxygen at 1573 K over the composition range $1.67 \leq O/Ti \leq 2.0$.
[42]	High temperature microcalorimetry, CO/CO_2 gas equilibration, thermogravimetry	Oxygen potential at 1323 K within the whole homogeneity range of rutile phase, TiO_{2-x}.
[43]	Calorimetric measurements	Partial molar enthalpy of mixing of oxygen at 1323 K for compositions $O/Ti < 0.6$.
[44]	Calorimetric measurements	Partial molar enthalpy of mixing of oxygen at 1323 K for compositions $0 \leq O/Ti \leq 1.0$.
[45]	Calorimetric measurements	Enthalpy of formation of *hcp* solid solutions at 298 K.
[46]	Calorimetric measurements	Enthalpy of formation of *hcp* solid solutions at 298 K.
[47]	Equilibration method (for investigations near to pure metal, i.e., at $p_{O_2} < 10^{-40}$), vacuum fusion method	Partial Gibbs energy of oxygen in various titanium–oxygen alloys equilibrated with calcium, magnesium and barium mixed with its respective oxides between 1173 and 1523 K.
[48]	Equilibration method	Partial molar Gibbs energy of oxygen in *bcc* titanium–oxygen alloys equilibrated with calcium and calcium oxide between 1173 and 1373 K.
[49]	Equilibration method	Partial molar Gibbs energy of oxygen in *bcc* titanium–oxygen alloys equilibrated with alkaline-earth metals in the temperature range 1300–1600 K.
[50]	Equilibration method	Partial molar Gibbs energy of oxygen in *bcc and hcp* titanium–oxygen alloys equilibrated with alkaline-earth metals in temperature range 1150–1600 K.
[51]	Equilibration method	Partial molar Gibbs energy of oxygen in *hcp* titanium–oxygen alloys up to 30 at.% oxygen equilibrated with alkaline-earth metal vapor of known partial pressure and solid alkaline-earth metal oxides between 1073 and 1273 K.
[52]	CO/CO_2 gas equilibration, thermogravimetry	Partial pressure of oxygen over the non-stoichiometric TiO_{2-x} between 1200 and 1500 K.
[53]	CO/CO_2 gas equilibration, thermogravimetry	Partial pressure of oxygen over the non-stoichiometric TiO_{2-x} between 1207 and 1467 K.
[54]	H_2/H_2O gas equilibration	Activities of Ti at 1073 K.
[55]	CO/CO_2 gas equilibration, thermogravimetry	Partial pressure of oxygen over the non-stoichiometric TiO_{2-x} between 1273 and 1373 K.
[56]	CO(g)/C(s) equilibration, thermogravimetry	Oxygen potentials over the oxide phase mixtures $Ti_2O_3 + Ti_3O_5$ and $Ti_3O_5 + Ti_4O_7$ in the temperature range 1180–1330 K.

Table 2 (*continued*)

Ref.	Experimental technique	Measured quantity, temperatures, compositions
[57]	Electrical resistivity measurements, CO/CO_2 and H_2/H_2O buffer equilibration	Oxygen potentials near the boundary of the homogeneity range of rutile as well as in titanium oxides in the composition range from Ti_3O_5 to Ti_6O_{11} between 1273 and 1773 K.
[58]	H_2–He gas (of controlled H_2O content) equilibration, thermogravimetry	Partial pressure of oxygen in equilibrium with different compositions of non-stoichiometric rutile TiO_{2-x} between 1273 and 1623 K.
[59]	H_2/H_2O gas equilibration, thermogravimetry	Equilibrium oxygen pressure over titanium oxides in the composition range from Ti_4O_7 to Ti_6O_{11} between 1323 and 1423 K.
[60]	CO_2/H_2 and CO/CO_2 gas equilibration, thermogravimetry	Oxygen fugacities over the two-phase regions of adjacent Magneli phases Ti_nO_{2n-1} ($3 \leq n \leq 10$) to non-stoichiometric rutile between 1473 and 1973 K.
[61]	H_2/H_2O gas equilibration, thermogravimetry	Oxygen potential over titanium oxides in the composition range from Ti_3O_5 to the non-stoichiometric rutile at 1304 K.
[62]	Knudsen effect	Vapor pressure of TiO(g) over solid titanium monoxide in the temperature range 1850–2050 K.
[63]	Knudsen effect	Vapor pressure of TiO(g) for the $Ti_2O_3 + Ti_3O_5$ equilibrium in the temperature range 1930–2050 K.
[64]	Knudsen effect, mass spectrometry	Potentials of Ti(g) and TiO(g) over stoichiometric titanium monoxide in the temperature range 1700–1900 K.
[65]	Mass spectrometry	Vapor pressure of TiO(g) over the whole range of homogeneity of titanium monoxide at 1800 K, vapor pressure of TiO(g) over stoichiometric titanium monoxide in the temperature range 1693–1895 K.
[66]	Multiple cell mass spectrometry	Activity of Ti, TiO and TiO_2 in the temperature range 1700–2200 K in the solid Ti_2O–TiO_2 and liquid Ti_2O_3–TiO_2 pseudobinary systems.
[67]	Mass spectrometry coupled with multiple Knudsen effusion cell	Activity of Ti and TiO in the temperature range 1650–1970 K over the compositions $0.47 \leq O/Ti \leq 1.396$.

Only data which were used in the present assessment are given.

have crystal structures derived from rutile by crystallographic shear. The maximum value of n is not known exactly. It was estimated to be 28 by Jacob et al. [41] based on investigated composition of a phase which was in equilibrium with TiO_{2-x}, while Roy and White [60] suggested that discrete equilibrium phases exist for $n \leq 99$. In the previous assessments, Magneli phases were taken into account up to $n = 20$ [11–13].

After the assessment of Waldner and Eriksson [13] a thermodynamic study of TiO_x ($1.67 \leq x \leq 2.0$) at 1573 K was published by Jacob et al. [41] using a combination of thermogravimetry and the EMF technique. Measured oxygen partial pressures at 1573 K versus x in TiO_x show reasonable agreement with the data of Zador and Alcock [31] in the stability domain of rutile and for Magneli phases with $n < 6$. For the intermediate values of x, the chemical potentials of oxygen reported by Zador and Alcock [31] are more positive, while the oxygen potentials reported by Suzuki and Sambongi [29] are significantly more positive than those obtained by Jacob et al. [41] in the whole range of x.

3. Thermodynamic modeling

The Gibbs energy functions of all phases are referred to the enthalpy of pure elements in their stable states at 298.15 K and 1 bar pressure (stable element reference H^{SER}). Gibbs energy functions of the pure elements are taken from the SGTE (Scientific Group Thermodata Europe) unary database [68], while the description of the stoichiometric phases, α-TiO and Magneli phases ($n \leq 20$) is adopted from the SGTE substance database [69] and the assessment of Waldner and Eriksson [13], respectively. The Gibbs energy functions of the pure elements, stoichiometric solid phases and end-members of solutions are given by

$$^{\circ}G(T) = G(T) - H^{SER} = a + bT + cT\ln(T) + dT^2 + eT^3 + f/T + \sum_n g_n T^n, \quad (1)$$

where a to f and g_n are coefficients and n stands for a set of integers.

The gas phase is described as an ideal mixture containing the species Ti, TiO, TiO_2, O, O_2 and O_3. The Gibbs energy of the gas phase is given as

$$G^{gas} = \sum_i x_i\, {}^{\circ}G_i^{gas} + RT\sum_i x_i \ln x_i + RT\ln(P/P_0), \quad (2)$$

where x_i is the mole fraction of the species i in the gas phase, $^{\circ}G_i^{gas}$ is the standard Gibbs energy of the gaseous species i [69], R is the gas constant, and P_0 is the standard pressure of 1 bar.

Both *bcc* and *hcp* solid solutions of Ti are considered to dissolve oxygen interstitially. Oxygen solubility in the *bcc* and *hcp* phases is represented by a two-sublattice model based on the compound energy formalism [70] with one sublattice fully occupied by Ti and the other one occupied with oxygen and vacancies, i.e., $(Ti)_1(O, Va)_u$. The stoichiometry u of the oxygen sublattice is based on the number of occupied interstitial sites per titanium atom. The oxygen atoms are located in the octahedral voids of *hcp*-Ti [71], and thus there is one interstitial site per titanium atom. However, two neighbouring octahedral sites along the hexagonal c-axis are unlikely to be occupied simultaneously. Therefore, the

stoichiometry of $u = 1/2$ is more realistic for describing the maximum oxygen solubility in *hcp*-Ti. Although the location of oxygen atoms in *bcc*-Ti is not clearly defined, it is likely that they also occupy octahedral voids. Structurally, there are three interstitial octahedral sites per titanium atom, but obviously all these sites cannot be available to oxygen atoms. It is related to the fact that the occupation of an interstitial site is prevented by the prior occupation of a neighbouring interstitial site, since effective repulsion exists between the near-neighbour O-atoms. Considering the symmetry, three interstitial sublattices can be identified when different planes (001, 110, or 001) are occupied and the general formula would be $(Ti)_1(O, Va)_1(O, Va)_1(O, Va)_1$. Maximum separation is achieved, however, if only one sublattice is occupied and the two others remain vacant, i.e., $(Ti)_1(O, Va)_1(Va)_1(Va)_1$, which is exactly the model for the *bcc* phase employed in the present work. This would result in a tetragonal distortion, which is usually not possible to check experimentally because the oxygen solubility is much too low. The second reason is to avoid the possible stabilization of the hypothetical TiO_3 compound. For any metal–oxygen (M–O) system the dissolution of oxygen is the metal lattice results in the substantial loss of entropy, so that the enthalpy of formation of the MO_3 end-member should be given a large negative value. The molar Gibbs energy of *hcp* and *bcc* solid solutions is given by

$$G^{\varphi} = y_{Va}\,{}^{\circ}G^{\varphi}_{Ti:Va} + y_O\,{}^{\circ}G^{\varphi}_{Ti:O} + uRT(y_{Va}\ln y_{Va} + y_O \ln y_O) + {}^{E}G^{\varphi}. \quad (3)$$

The excess Gibbs energy is expressed by the Redlich–Kister polynomials [72]:

$${}^{E}G^{\varphi} = y_O y_{Va} \sum_{\nu=0}^{n} {}^{\nu}L^{\varphi}_{Ti:O,Va}(y_O - y_{Va})^{\nu}, \quad (4)$$

where ${}^{\circ}G^{\varphi}_{Ti:Va}$ and ${}^{\circ}G^{\varphi}_{Ti:O}$ are the expressions for the Gibbs energy of the pure *bcc*-Ti or *hcp*-Ti, and the hypothetical compounds TiO and 1/2 Ti_2O with *bcc* or *hcp* arrangements of titanium atoms, respectively.

Stoichiometric titanium dioxide in its stable modification (rutile) has a structure with two atomic positions in the unit cell, one for Ti^{4+} (2a) and one for O^{2-} (4f). Non-stoichiometric rutile has an O/Ti ratio less than two. The nature of the defect structure in TiO_{2-x} is not yet fully understood and there is some controversy in the literature. The experimental data suggest the existence of either doubly charged oxygen vacancies and free electrons [31,33,41,52,53,55] or their combination with interstitially dissolved titanium Ti^{3+} ions [30,40,42]. In the present work, the oxygen vacancy model is preferred. The lack of negative charge in the anion sublattice due to oxygen vacancies is effectively compensated by substitution of Ti^{3+} for Ti^{4+} in the cation sublattice. The non-stoichiometry of rutile can then be expressed as $(Ti^{4+}, Ti^{3+})_1(O^{2-}, Va)_2$, and the molar Gibbs energy is defined as

$$G^{TiO_{2-x}} = y_{Ti^{4+}}y_{O^{2-}}\,{}^{\circ}G_{Ti^{4+}:O^{2-}} + y_{Ti^{3+}}y_{O^{2-}}\,{}^{\circ}G_{Ti^{3+}:O^{2-}} + y_{Ti^{4+}}y_{Va}\,{}^{\circ}G_{Ti^{4+}:Va} + y_{Ti^{3+}}y_{Va}\,{}^{\circ}G_{Ti^{3+}:Va}$$

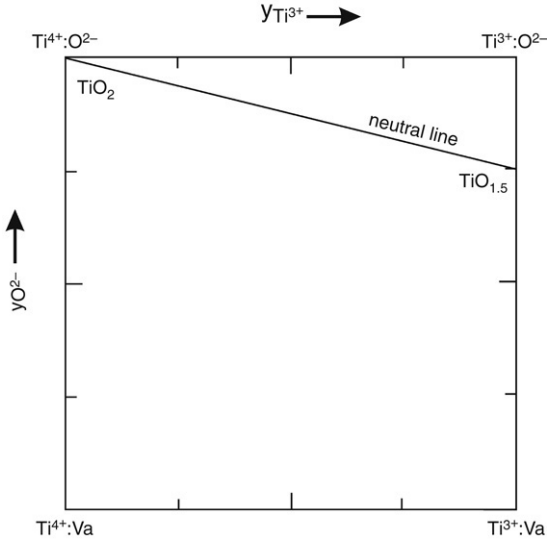

Fig. 1. Geometric representation of thermodynamic model for non-stoichiometric rutile.

$$+ RT\left(y_{Ti^{4+}}\ln y_{Ti^{4+}} + y_{Ti^{3+}}\ln y_{Ti^{3+}}\right) + 2RT\left(y_{O^{2-}}\ln y_{O^{2-}} + y_{Va}\ln y_{Va}\right) + {}^{E}G^{TiO_{2-x}}. \quad (5)$$

Due to the narrow non-stoichiometry range of rutile, the excess term ${}^{E}G^{TiO_{2-x}}$ is set equal to zero in this assessment. The ${}^{\circ}G$-terms correspond to the Gibbs energies of the different compounds formed by considering only one species in each sublattice. The model is shown by the composition square in Fig. 1. The neutral end-member, ${}^{\circ}G_{Ti^{4+}:O^{2-}}$, corresponds to stoichiometric rutile while the other three end-members, i.e., corners of the composition square, correspond to unphysical compounds with a net charge. The neutral compound $TiO_{1.5}$ with the rutile-related structure (Fig. 1), which is obtained by the combination of $(Ti^{3+})(O^{2-})_2$ and $(Ti^{3+})(Va)_2$, has the molar Gibbs energy

$${}^{\circ}G_{TiO_{1.5}} = \frac{1}{2}\,{}^{\circ}G_{R-Ti_2O_3} = \frac{3}{4}\,{}^{\circ}G_{Ti^{3+}:O^{2-}} + \frac{1}{4}\,{}^{\circ}G_{Ti^{3+}:Va} + 2RT\left(\frac{3}{4}\ln\frac{3}{4} + \frac{1}{4}\ln\frac{1}{4}\right), \quad (6)$$

where the last term is due to the ideal entropy of mixing in the anion sublattice. The additional two end-members are defined by Eqs. (7) and (8):

$${}^{\circ}G_{Ti^{4+}:Va} = {}^{\circ}G_{TiO_2} - {}^{\circ}G_{O_2(g)} \quad (7)$$

$${}^{\circ}G_{Ti^{4+}:O^{2-}} + {}^{\circ}G_{Ti^{3+}:Va} = {}^{\circ}G_{Ti^{4+}:Va} + {}^{\circ}G_{Ti^{3+}:O^{2-}} \quad (8)$$

where the first term ${}^{\circ}G_{Ti^{4+}:Va}$ (Eq. (7)) is chosen to be the reference and the second one, ${}^{\circ}G_{Ti^{3+}:Va}$, is determined using the reciprocal relation.

Although non-stoichiometric TiO_x exhibits several structural modifications [1], experimental phase equilibrium and thermodynamic data are confined to the high-temperature γ-TiO_x. The

latter has a rocksalt-type structure with two sublattices, but the simplest model $(Ti, Va)_1(O, Va)_1$ used by Pajunen and Kivilahti [8] is unable to describe the increase of lattice constant with increasing metal content, a fact which is supported by various studies compiled by Murray and Wriedt [1]. A more advanced two-sublattice definition based on the bond energy formalism $(Ti^{2+}, Va^{2+})_1(O^{2-}, Va^{2-})_1$ was successfully applied for the modeling of the TiO_x phase [13], but unfortunately, this model is currently incorporated only into the ChemSage software package. Therefore, the $(Ti^{2+}, Ti^{3+}, Va)_1(Ti, Va)_1(O^{2-})_1$ model used by Lee [9] and Lee and Saunders [10] is adopted in the present work. It is based on the compound energy formalism (CEF), which is compatible with most of commercial software for thermodynamic calculations and can adequately describe the deviations from stoichiometric composition towards both the Ti-side and the O-side by the introduction of neutral Ti atoms in the interstitial sites and by the introduction of Ti^{3+} ions and vacancies in the cation sublattice. In addition, this model accounts for the observed increase of the lattice constant of the TiO_x phase with increasing titanium content [9,10]. Neglecting the oxygen vacancies does not necessarily contradict the experimental data, since only the densities and the lattice parameters were measured [1]. The molar Gibbs energy is defined as

$$\begin{aligned} G^{\mathrm{TiO}_x} = {} & y_{\mathrm{Ti}^{2+}} y_{\mathrm{Ti}} {}^{\circ}G_{\mathrm{Ti}^{2+}:\mathrm{Ti}:\mathrm{O}^{2-}} + y_{\mathrm{Ti}^{3+}} y_{\mathrm{Ti}} {}^{\circ}G_{\mathrm{Ti}^{3+}:\mathrm{Ti}:\mathrm{O}^{2-}} \\ & + y'_{\mathrm{Va}} y_{\mathrm{Ti}} {}^{\circ}G_{\mathrm{Va}:\mathrm{Ti}:\mathrm{O}^{2-}} + y_{\mathrm{Ti}^{2+}} y''_{\mathrm{Va}} {}^{\circ}G_{\mathrm{Ti}^{2+}:\mathrm{Va}:\mathrm{O}^{2-}} \\ & + y_{\mathrm{Ti}^{3+}} y''_{\mathrm{Va}} {}^{\circ}G_{\mathrm{Ti}^{3+}:\mathrm{Va}:\mathrm{O}^{2-}} + y'_{\mathrm{Va}} y''_{\mathrm{Va}} {}^{\circ}G_{\mathrm{Va}:\mathrm{Va}:\mathrm{O}^{2-}} \\ & + RT(y_{\mathrm{Ti}^{2+}} \ln y_{\mathrm{Ti}^{2+}} + y_{\mathrm{Ti}^{3+}} \ln y_{\mathrm{Ti}^{3+}} + y'_{\mathrm{Va}} \ln y'_{\mathrm{Va}}) \\ & + RT(y_{\mathrm{Ti}} \ln y_{\mathrm{Ti}} + y''_{\mathrm{Va}} \ln y''_{\mathrm{Va}}) + {}^{E}G^{\mathrm{TiO}_x} \end{aligned} \tag{9}$$

where

$$\begin{aligned} {}^{E}G^{\mathrm{TiO}_x} = {} & y_{\mathrm{Ti}^{2+}} y_{\mathrm{Ti}^{3+}} y_{\mathrm{Ti}} L_{\mathrm{Ti}^{2+},\mathrm{Ti}^{3+}:\mathrm{Ti}:\mathrm{O}^{2-}} \\ & + y_{\mathrm{Ti}^{2+}} y'_{\mathrm{Va}} y_{\mathrm{Ti}} L_{\mathrm{Ti}^{2+},\mathrm{Va}:\mathrm{Ti}:\mathrm{O}^{2-}} \\ & + y_{\mathrm{Ti}^{3+}} y'_{\mathrm{Va}} y_{\mathrm{Ti}} L_{\mathrm{Ti}^{3+},\mathrm{Va}:\mathrm{Ti}:\mathrm{O}^{2-}} \\ & + y_{\mathrm{Ti}^{2+}} y_{\mathrm{Ti}^{3+}} y''_{\mathrm{Va}} L_{\mathrm{Ti}^{2+},\mathrm{Ti}^{3+}:\mathrm{Va}:\mathrm{O}^{2-}} \\ & + y_{\mathrm{Ti}^{2+}} y'_{\mathrm{Va}} y''_{\mathrm{Va}} L_{\mathrm{Ti}^{2+},\mathrm{Va}:\mathrm{Va}:\mathrm{O}^{2-}} \\ & + y_{\mathrm{Ti}^{3+}} y'_{\mathrm{Va}} y''_{\mathrm{Va}} L_{\mathrm{Ti}^{3+},\mathrm{Va}:\mathrm{Va}:\mathrm{O}^{2-}} \\ & + y_{\mathrm{Ti}^{2+}} y_{\mathrm{Ti}} y''_{\mathrm{Va}} L_{\mathrm{Ti}^{2+}:\mathrm{Ti},\mathrm{Va}:\mathrm{O}^{2-}} \\ & + y_{\mathrm{Ti}^{3+}} y_{\mathrm{Ti}} y''_{\mathrm{Va}} L_{\mathrm{Ti}^{3+}:\mathrm{Ti},\mathrm{Va}:\mathrm{O}^{2-}} \\ & + y'_{\mathrm{Va}} y_{\mathrm{Ti}} y''_{\mathrm{Va}} L_{\mathrm{Va}:\mathrm{Ti},\mathrm{Va}:\mathrm{O}^{2-}} \end{aligned} \tag{10}$$

and y'_{Va} and y''_{Va} correspond to the vacancies in the first and second sublattice, respectively. Only the $L_{\mathrm{Ti}^{2+}:\mathrm{Ti},\mathrm{Va}:\mathrm{O}^{2-}}$ interaction parameter is optimized in the present work (Table 3), while others are fixed with zero.

The associate solution model [73–78] is widely used for the description of thermodynamic properties of liquids. There are differences between the authors in the way in which the excess terms are handled, but all consider that some type of complex or associate is formed in the liquid by the reaction between the components of the system. The thermodynamic properties of the liquid then depend predominantly on the Gibbs energy of formation of these associates rather than on interaction between components of the system. The thermodynamic properties of the liquid in systems with compound formation tendency show, in most cases, strong deviation from the ideal mixing behaviour, which is caused by the existence of chemical short-range ordering (CSRO). This gives rise to an enthalpy of mixing diagram which is characterized by sharp changes at critical compositions, where the associates exist, and also by markedly non-ideal entropies of mixing. The short-range ordered volume parts are summarily described as associates with well defined compositions, while the remaining atoms are regarded as being randomly distributed. The associates are in a steady dynamic equilibrium with the non-associated atoms, which is governed by the mass action law.

The (Ti, O, TiO, $TiO_{1.5}$, TiO_2) model was chosen for description of liquid in the present work. The equilibrium reaction between the species in the liquid phase is given by

$$\mathrm{Ti} + j\mathrm{O} = \mathrm{TiO}_j \tag{11}$$

with $j = 1$, 1.5, and 2. The Gibbs energy of the liquid is then

$$\begin{aligned} G^{\mathrm{liq}} = {} & x_{\mathrm{Ti}} {}^{\circ}G_{\mathrm{Ti}} + x_{\mathrm{O}} {}^{\circ}G_{\mathrm{O}} + \sum_j x_{\mathrm{TiO}_j} {}^{\circ}G_{\mathrm{TiO}_j} \\ & + RT\left(x_{\mathrm{Ti}} \ln x_{\mathrm{Ti}} + x_{\mathrm{O}} \ln x_{\mathrm{O}} + \sum_j x_{\mathrm{TiO}_j} \ln x_{\mathrm{TiO}_j}\right) \\ & + {}^{E}G^{\mathrm{liq}}_{\mathrm{ass}}, \end{aligned} \tag{12}$$

where x_{Ti}, x_{O} and x_{TiO_j} are the mole fractions of the assumed species.

The excess Gibbs energy ($^{E}G^{\mathrm{liq}}_{\mathrm{ass}}$) is given by the general formula using the Redlich–Kister polynomial:

$${}^{E}G^{\mathrm{liq}}_{\mathrm{ass}} = x_i x_j \sum_{\nu=0}^{n} {}^{\nu}L^{\mathrm{liq}}_{i,j}(x_i - x_j)^{\nu}, \tag{13}$$

where i and j correspond to the species Ti, O, TiO, $TiO_{1.5}$, and TiO_2. The binary interaction parameters are described as linear functions of temperature, i.e., ${}^{\nu}L^{\mathrm{liq}}_{i,j} = a_\nu + b_\nu T$.

4. Results and discussion

The optimized thermodynamic parameters are compiled in Table 3. Fig. 2 shows calculated and experimental partial pressures of oxygen over the unsaturated solid solution of oxygen in *bcc* titanium. In addition to the EMF measurements by Reznichenko and Khalimov [34], equilibria of titanium alloys with alkaline-earth metal/metal–oxide mixtures were investigated by Kubaschewski and Dench [47], Miyazaki et al. [50], Okabe et al. [48] and Sano and Tsukihashi [49]. The method was first adopted in Ref. [47] and the partial pressure of oxygen in the case of *bcc* solid solution was determined using Ca/CaO equilibrium. The solubility of calcium in titanium was reported to be very small, about 60 mass ppm at 1273 K [79], so the Ti–O alloys in equilibrium with calcium and calcium oxides behave just as in the Ti–O binary system.

Table 3
Summary of the thermodynamic parameters describing condensed phases in the Ti–O system referred to stable element reference H^{SER} ($T = 298.15$ K, $P = 1$ bar)

Phase, parameter	Ref.
Liquid (Ti, TiO, $TiO_{3/2}$, TiO_2, O), Eqs. (11)–(13)	
${}^{\circ}G^{liq}_{TiO_2} = 61\,022.4 - 28.2T + {}^{\circ}G_{TiO_2}$	This work
${}^{\circ}G^{liq}_{TiO_{3/2}} = 57\,073.7 - 22.8T + 0.5\,{}^{\circ}G_{Ti_2O_3}$	This work
${}^{\circ}G^{liq}_{TiO} = 77671.8 - 30.7T + {}^{\circ}G_{Ti_1O_1}$	This work
${}^{\circ}G^{liq}_{Ti}$, ${}^{\circ}G^{liq}_{O}$	[68]
${}^{0}L^{liq}_{Ti,TiO} = 121\,427.1 - 73.4T$	This work
${}^{1}L^{liq}_{Ti,TiO} = -77\,733.9 + 41.9T$	This work
${}^{0}L^{liq}_{TiO_{3/2},TiO_2} = -19\,200.8$	This work
${}^{1}L^{liq}_{TiO_{3/2},TiO_2} = 100\,402.4 - 48.6T$	This work
bcc$(Ti)_1(O, Va)_1$, Eqs. (3) and (4)	
${}^{\circ}G^{bcc}_{Ti:Va} = {}^{\circ}G_{Ti(bcc)}$	[68]
${}^{\circ}G^{bcc}_{Ti:O} = -511\,601 + 83.1777T + {}^{\circ}G_{Ti(hcp)} + 1/2\,{}^{\circ}G_{O_2(g)}$	This work
${}^{\circ}L^{bcc}_{Ti:O,Va} = -24\,574.9$	This work
hcp$(Ti)_1(O, Va)_{0.5}$, Eqs. (3) and (4)	
${}^{\circ}G^{bcc}_{Ti:Va} = {}^{\circ}G_{Ti(hcp)}$	[68]
${}^{\circ}G^{hcp}_{Ti:O} = -277\,514 + 40.6543T + {}^{\circ}G_{Ti(hcp)} + 1/4\,{}^{\circ}G_{O_2(g)}$	This work
${}^{\circ}L^{hcp}_{Ti:O,Va} = 817.9$	This work
TiO_x $(Ti^{3+}, Ti^{2+}, Va)_1(Ti, Va)_1(O^{2-})_1$, Eqs. (9) and (10)	
${}^{\circ}G^{TiO_x}_{Ti^{2+}:Ti:O^{2-}} = -554\,987.5 + 84.614T + 2\,{}^{\circ}G_{Ti(hcp)} + 1/2\,{}^{\circ}G_{O_2(g)}$	This work
${}^{\circ}G^{TiO_x}_{Ti^{3+}:Ti:O^{2-}} = -560\,666.4 + 84.614T + 2\,{}^{\circ}G_{Ti(hcp)} + 1/2\,{}^{\circ}G_{O_2(g)}$	This work
${}^{\circ}G^{TiO_x}_{Va:Ti:O^{2-}} = {}^{\circ}G_{Ti_1O_1} + 200\,000$	This work
${}^{\circ}G^{TiO_x}_{Ti^{2+}:Va:O^{2-}} = {}^{\circ}G_{Ti_1O_1} + 6605.4 + 7.7366T$	This work
${}^{\circ}G^{TiO_x}_{Ti^{3+}:Va:O^{2-}} = 1/2\,{}^{\circ}G_{Ti_2O_3} + 5494.9 + 10.2103T$	This work
${}^{\circ}G^{TiO_x}_{Va:Va:O^{2-}} = 0$	This work
${}^{\circ}L^{TiO_x}_{Ti^{2+}:Ti,Va:O^{2-}} = 17\,092.5 - 3.8448T$	This work
Rutile $(Ti^{3+}, Ti^{4+})_1$ $(O^{2-}, Va)_2$, Eqs. (5)–(8)	
${}^{\circ}G^{rut}_{Ti^{4+}:Va} = {}^{\circ}G_{TiO_2} - {}^{\circ}G_{O_2(g)}$	This work
${}^{\circ}G^{rut}_{Ti^{4+}:O^{2-}} = -976\,986.6 + 484.74037T - 77.76175T\ln T - 67\,156\,800T^{-2} + 1683\,920T^{-1}$ (298.15–4000 K)	[13]
${}^{\circ}G^{rut}_{Ti^{3+}:Va} = 1/2\,{}^{\circ}G_{Ti_2O_3} - 3/4\,{}^{\circ}G_{O_2(g)} + 9.35T + 55\,781.5 - 4.0852T$	This work
${}^{\circ}G^{rut}_{Ti^{3+}:O^{2-}} = 1/2\,{}^{\circ}G_{Ti_2O_3} + 1/4\,{}^{\circ}G_{O_2(g)} + 9.35T + 55\,781.5 - 4.0852T$	This work
${}^{\circ}G_{\alpha\text{-}TiO} = {}^{\circ}G_{Ti_1O_1} + 7867.689 + 0.9302T$	This work
${}^{\circ}G_{Ti_1O_1} = -551\,056.766 + 327\,015.164T^{-1} + 252.169378T - 41.994808T\ln T + 0.00889792452T^2 + 1.0970448\times10^{-8}T^3$ (298.15–2500 K)	[9]
${}^{\circ}G_{Ti_3O_2} = 3\,{}^{\circ}G_{Ti(hcp)} + {}^{\circ}G_{O_2(g)} - 1108\,030.7 + 195.8524T$	This work
${}^{\circ}G_{Ti_4O_7} = -346\,1530 + 2504.7933T - 364.36711T\ln T - 8443.569T^{0.5} + 1259\,760T^{-1} + 24\,091\,400T^{-2}$	This work
${}^{\circ}G_{Ti_5O_9} = -4438\,624 + 2987.3392T - 442.20473T\ln T - 8443.569T^{0.5} + 2943\,680T^{-1} - 4306\,5400T^{-2}$	This work
${}^{\circ}G_{Ti_7O_{13}} = -6393\,201 + 3954.5637T - 597.87990T\ln T - 8443.569T^{0.5} + 6311\,520T^{-1} - 177\,379\,000T^{-2}$	This work
${}^{\circ}G_{Ti_2O_3} = -1543\,640 + 185.96227T - 30.3934128T\ln T - 0.099958898T^2 - 5.93279345\times10^{-6}T^3 - 117\,799.056T^{-1}$ (298.15–470 K)	[13]
$= -1585\,377.8 + 937.087T - 147.673862T\ln T - 0.00173711312T^2 - 1.53383348\times10^{-10}T^3 + 2395\,423.68T^{-1}$ (470–2115 K)	
${}^{\circ}G_{Ti_3O_5} = -2492\,980 - 73.26557T + 23.9073342T\ln T - 0.420155188T^2 + 1.34740141\times10^{-4}T^3$ (298.15–450 K)	[13]
$= -2508\,055.23 + 925.801T - 158.99208T\ln T - 0.0251T^2$ (450–5000 K)	
${}^{\circ}G_{Ti_6O_{11}}$, ${}^{\circ}G_{Ti_8O_{15}}$, ${}^{\circ}G_{Ti_9O_{17}}$, ${}^{\circ}G_{Ti_{10}O_{19}}$, ${}^{\circ}G_{Ti_{20}O_{39}}$	[13]

Values are given in SI units (joule, mole, and kelvin).

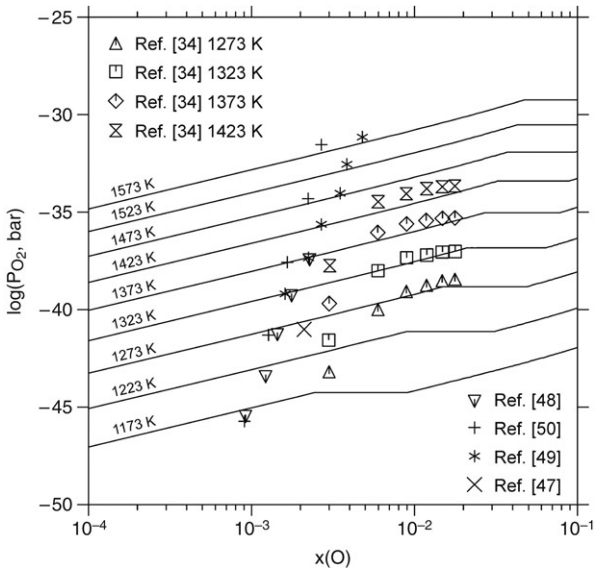

Fig. 2. Calculated and experimental partial pressures of oxygen over the unsaturated solid solution of oxygen in *bcc* titanium. The temperatures in Refs. [47–50] are given by the numbers on the corresponding curves.

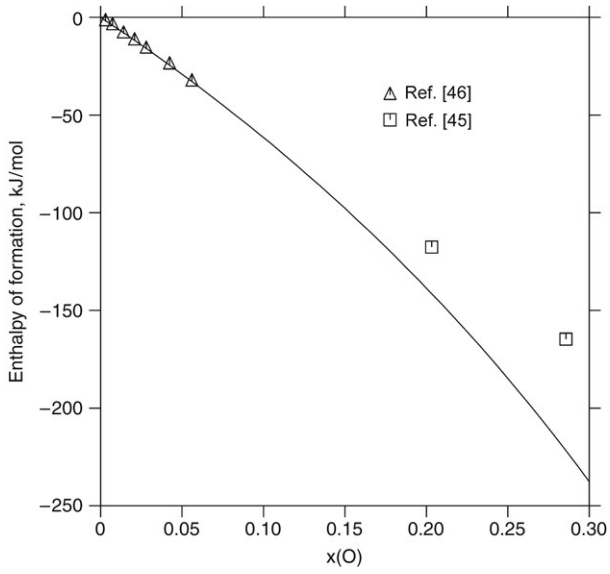

Fig. 4. Calculated enthalpies of formation of the *hcp* Ti–O solid solutions at 298 K together with the experimental data. The reference states are *hcp* Ti and O_2 gas.

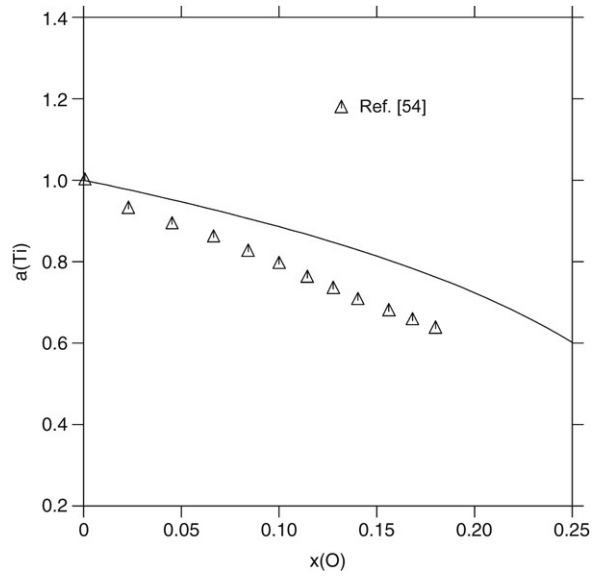

Fig. 3. Calculated activities of titanium in the *hcp* Ti–O solid solution at 1073 K along with the experimental data. The reference state is *hcp* Ti.

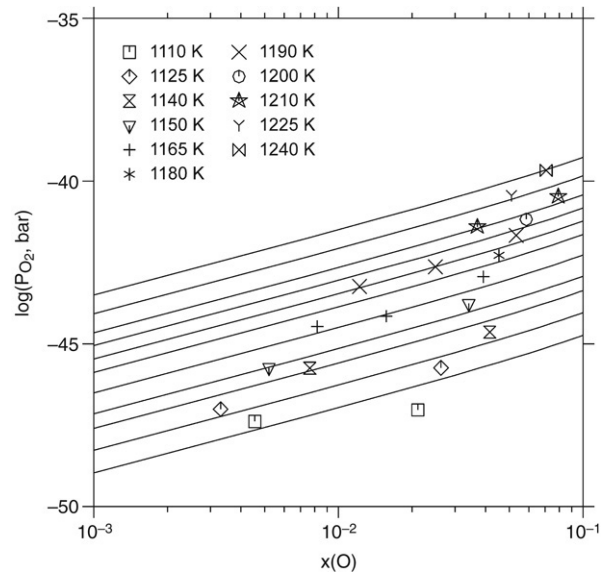

Fig. 5. Calculated and experimental [51] partial pressures of oxygen over the unsaturated solid solution of oxygen in *hcp* titanium up to 10 at.%. The curves are calculated at temperatures shown in the legend.

In equilibrium, the partial pressure of oxygen over titanium alloy is equal to the partial pressure of oxygen given by the reaction $Ca(l,\ g) + 1/2O_2 = CaO(s)$. Agreement between calculated and experimental data is very good, though some discrepancy with the data of Ref. [34] exists at the lowest oxygen concentration.

The calculated activity of titanium in the *hcp* solid solutions is compared with experimental data of Hepworth and Schuhmann [54] in Fig. 3. The general trend is well reproduced, although some systematic deviations cannot be avoided to keep reasonable agreement with other datasets. Fig. 4 presents the calculated enthalpies of formation of *hcp* Ti–O alloys at 298 K together with the corresponding experimental data [45,46]. Agreement between calculated and measured values is very good for oxygen contents below 10 at.%. Fig. 5 shows the calculated equilibrium oxygen pressures over the unsaturated solid solution of oxygen in *hcp* titanium up to 10 at.% in comparison with experimental data reported by Komarek and Silver [51]. The titanium alloys were equilibrated with a Ca/CaO mixture. Again, the correspondence between calculations and experiments is very good, despite the increasing deviations at lower temperatures, probably because of the difficulties to reach the steady state. At higher oxygen

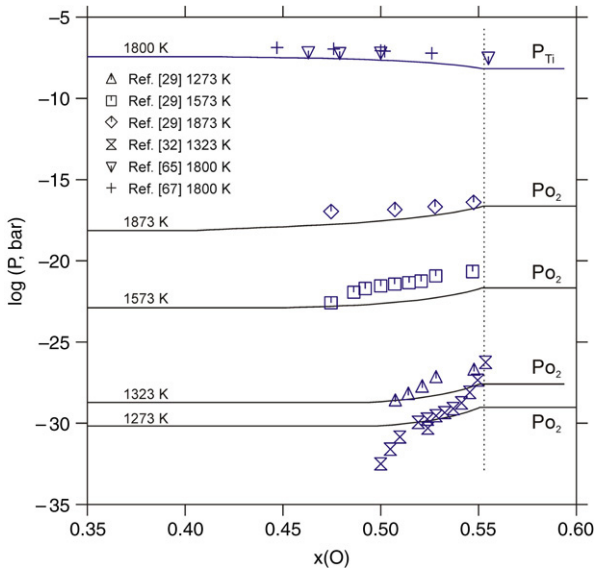

Fig. 6. Calculated partial pressures of oxygen and titanium over the TiO_x solid solution in comparison with experimental data. The dashed line corresponds to the TiO_x/Ti_2O_3 phase boundary.

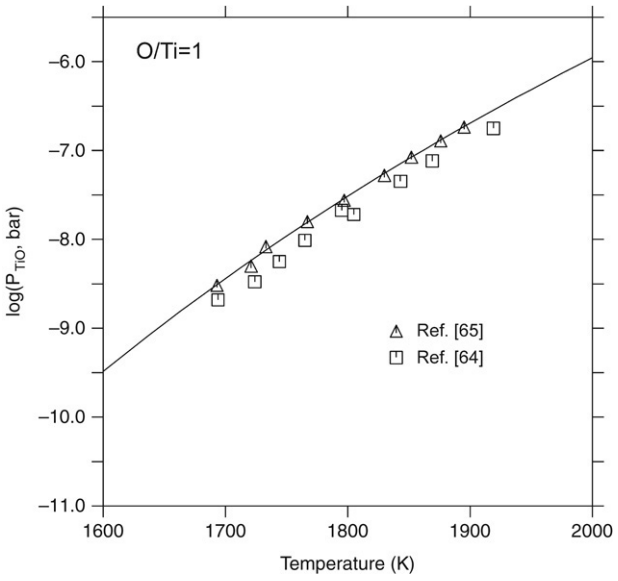

Fig. 7. Experimental and calculated TiO(g) partial pressures over the TiO_x solid solution at 50 at.% O.

contents, i.e., between 10 and 30 at.%, the equilibration with a Mg/MgO mixture [51] gave oxygen pressures which show a substantial discrepancy with the present calculations. Similar results were obtained in the previous assessment work [13]. The apparent differences between experimental and modeling results for this composition range (cf. Fig. 4) are likely due to the ordering phenomena, which cannot satisfactorily be described by the interstitial solution model. Indeed, ordered phases within the *hcp* domain, such as Ti_2O (α') [26,80], Ti_2O_{1-y} [81,82], Ti_3O [20,82,83], Ti_6O [20,84], and $Ti_{12}O$, were shown in various compilations [1,20,46,85–88] either as discrete compounds or as phases with wide homogeneity ranges produced from the disordered phases by second-order phase transitions [89,90]. The detailed placement of phase boundaries, however, is still very uncertain. For instance, they were shown as either persisting to the melting point [20,81,82, 85,91,92], or as disordering above 600 °C [46,84,88–90]. In the present work, such phases are not taken into account. In addition, the oxygen pressures obtained in equilibration with the Mg/MgO mixture show less reliability in comparison with the Ca/CaO mixture, because of the small weight changes of the samples caused by magnesium dissolution [51], while no weight changes were observed in the samples in contact with calcium.

Fig. 6 shows the calculated partial pressures of oxygen and titanium over the TiO_x solid solution together with experimental points. The calculated and measured values are in good agreement. At low temperatures (1273–1373 K), the experimental data [29,32] show considerable scatter, which is not surprising for the measurements of such low pressures. The effect of temperature on the partial pressure of TiO above the TiO_x solid solution at the stoichiometric composition (50 at.% oxygen) is shown in Fig. 7. Correspondence between calculations and experiments is good.

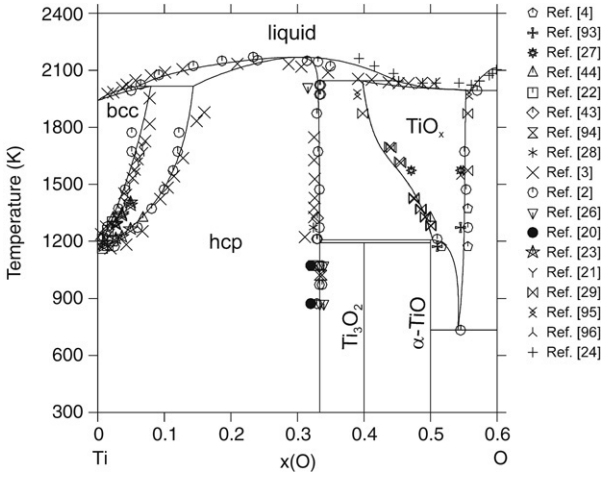

Fig. 8. Calculated Ti–O phase diagram up to 60 at.% O in comparison with experimental data [2–4,20–24,26–29,43,44,93–96].

Fig. 8 shows the phase diagram of the Ti–O system calculated up to 60 at.% of oxygen in the temperature range 300–2400 K for a total pressure of 1 bar in comparison with experimental data. It is evident that the present calculation is well consistent with most of the experimental information. Invariant equilibria involving all modeled phases in the Ti–O system are shown in Table 4 together with experimental information assessed by Murray and Wriedt [1].

The compound energy model used for rutile is able to give a good correspondence between calculated and measured partial pressures of oxygen within its homogeneity range (Figs. 9 and 10). As a result of optimization, the enthalpy and entropy of melting of TiO_2 are 67 404 J/mol of 31.47 J/(mol K), which can be compared to the values reported in JANAF tables [97] (calculated values): 68 000 J/mol, and 31.121 J/(mol K), respectively. The optimized congruent melting point of rutile is

Table 4
Calculated invariant reactions (second row) together with experimental information (first row) assessed by Murray and Wriedt [1]

Reaction	Temperature (K)	Composition (at.% O)		
liquid + hcp = bcc	1993 ± 25	5.00	13.00	8.00
	2016.42	6.05	14.34	7.98
hcp = liquid	2158 ± 25	~24	~24	
	2168.3	29.90	29.90	
liquid + hcp = TiO_x	2043	~55	31.40	34.5
	2043.7	44.87	33.07	39.79
liquid = $TiO_x + Ti_2O_3$	1993	~57	54.50	59.80
	1992.1	55.87	55.30	60.00
liquid = Ti_2O_3	2115 ± 10	60.00	60.00	
	2112.3	60.00	60.00	
liquid = $Ti_2O_3 + Ti_3O_5$	2043	63.00	60.20	62.25
	2039.7	61.98	60.00	62.25
Ti_3O_5 = liquid	–	–	–	
	2047.7	62.5	62.5	
liquid = $Ti_3O_5 + Ti_5O_9$	~1943	64.00	62.5	–
	1947.7	64.01	62.5	64.29
TiO_2 = liquid	2143	66.67	66.67	
	2142.3	66.62	66.62	
hcp + TiO_x = α-TiO	1213	33.30	51.00	50.00
	1208.6	33.33	50.28	50.00
hcp + α-TiO = Ti_3O_2	1193	32.40	50.00	40.00
	1193.0	33.33	50.00	40.00
TiO_x = α-TiO + Ti_2O_3	733	54.50	50.00	60.00
	733.5	54.11	50.00	60.00
$Ti_3O_5 + Ti_5O_9 = Ti_4O_7$	~1940	62.50	64.29	63.64
	1940.4	62.50	64.29	63.64
$Ti_3O_5 = Ti_2O_3 + Ti_4O_7$	<1000	62.50	60.00	63.64
	778.4	62.50	60.00	63.64

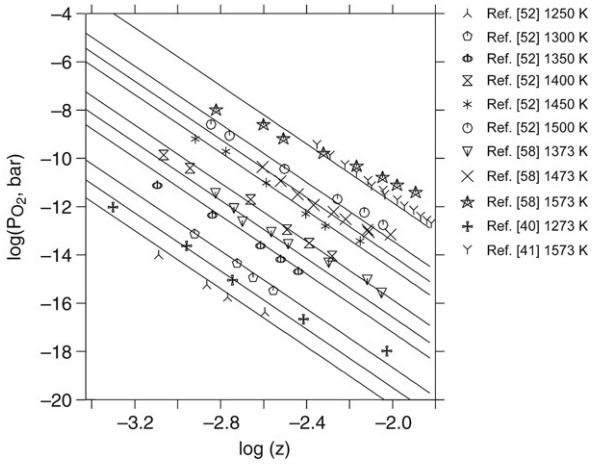

Fig. 9. Calculated partial pressures of oxygen within the homogeneity range of rutile TiO_{2-z} along with experimental points. The lines are calculated at temperatures shown in the legend.

2142.3 K (Table 4). The heat capacity of liquid TiO_2 is assumed to have the same temperature dependence as for the solid phase.

The phase diagram in the composition range between Ti_2O_3 and TiO_2 together with experimental data is presented

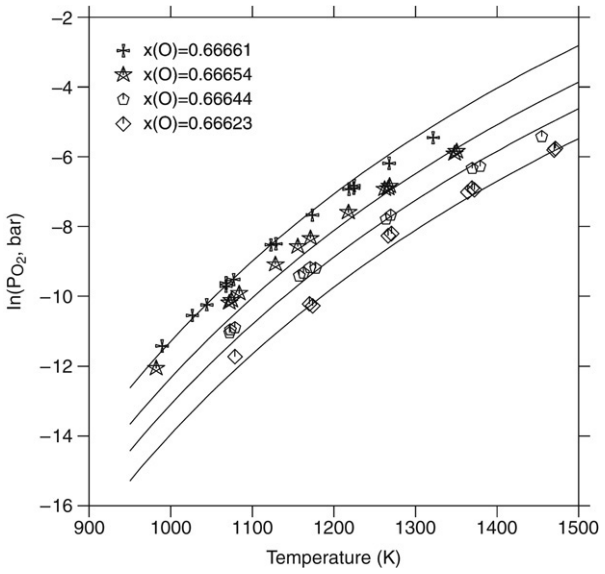

Fig. 10. Calculated partial pressures of oxygen versus temperature for fixed compositions of the non-stoichiometric rutile as compared with experimental measurements [40].

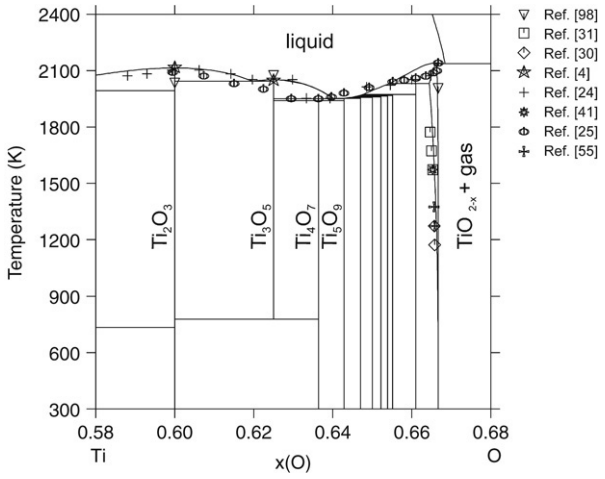

Fig. 11. Calculated Ti–O phase diagram in the composition range between Ti_2O_3 and rutile in comparison with experimental data [4,24,25,30,31,41,55,98].

in Fig. 11, while Fig. 12 shows in more detail a series of peritectic reactions involving Magneli phases. Predicted invariant equilibria in this composition range are given in Table 5. The descriptions of Magneli phases are taken from Ref. [13] and are very slightly modified for Ti_4O_7, Ti_5O_9 and Ti_7O_{13} to better fit the phase boundaries. Therefore, the calculated oxygen pressures in this region of the phase diagram are not significantly different from the corresponding plots in Ref. [13]. It should also be noted that the calculated phase diagrams (Figs. 8, 11 and 12) and invariant equilibria (Tables 4 and 5) are very similar to those already presented by Waldner and Eriksson [13]. Some minor differences originate from the different modeling of the liquid phase. Therefore, these calculated results are not discussed here in detail, but are intended to demonstrate the ability of the associate model to

Table 5
Predicted invariant reactions involving Magneli phases

Reaction	Temperature (K)	Composition (at.% O)		
liquid + Ti_6O_{11} = Ti_5O_9	1950.5	64.27	64.71	64.29
liquid + Ti_7O_{13} = Ti_6O_{11}	1954.7	64.43	65.00	64.71
liquid + Ti_8O_{15} = Ti_7O_{13}	1957.6	64.51	65.22	65.00
liquid + Ti_9O_{17} = Ti_8O_{15}	1962.4	64.61	65.39	65.22
liquid + $Ti_{10}O_{19}$ = Ti_9O_{17}	1965.6	64.67	65.52	65.39
liquid + $Ti_{20}O_{39}$ = $Ti_{10}O_{19}$	1971.3	64.76	66.10	65.52
liquid + TiO_{2-x} = $Ti_{20}O_{39}$	2030.4	65.43	66.44	66.10
liquid = TiO_{2-x} + gas	2138.6	66.84	66.63	99.99

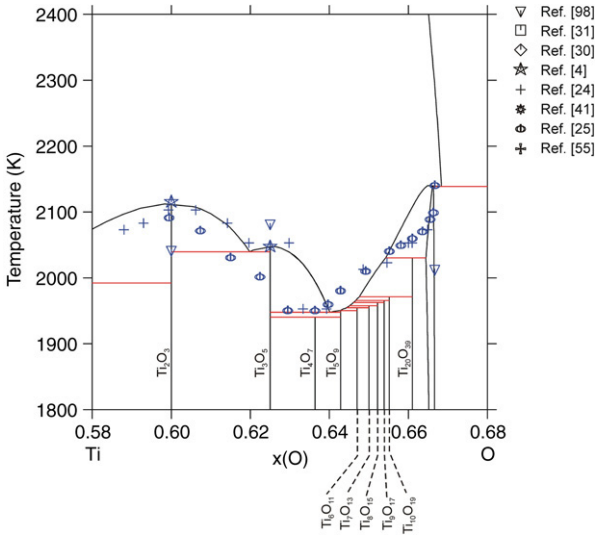

Fig. 12. Calculated Ti–O phase diagram showing in more detail a series of peritectic reactions involving Magneli phases in comparison with experimental data.

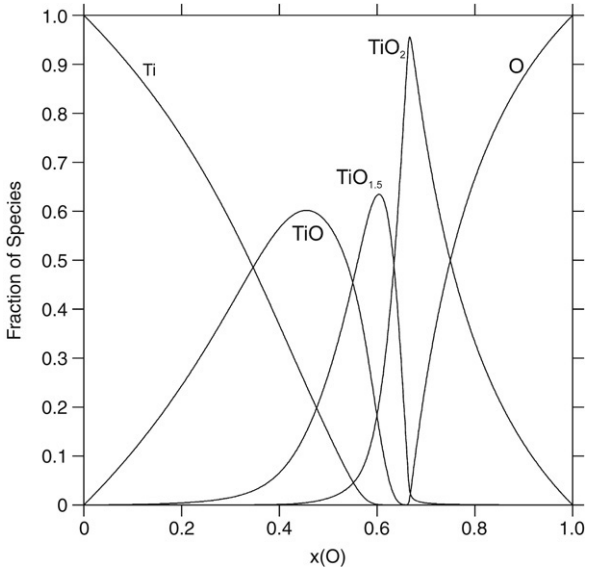

Fig. 13. Calculated species distribution in the liquid at 2150 K according to the present associate model.

describe phase equilibria in the Ti–O system. However, the liquid + rutile + gas equilibrium is predicted to be of eutectic type (Table 4) instead of the peritectic reaction calculated in Ref. [13].

The calculated fractions of different associates in the liquid phase at 2150 K are shown in Fig. 13. Waldner and Eriksson [13] published a similar diagram for the limited composition range (Ti–TiO_2) and mentioned the strong disproportionation of Ti^{3+} onto Ti^{2+} and Ti^{4+}. Their conclusion is confirmed in the present work, since the fraction of the $TiO_{1.5}$ species at the composition of 60 at.% O is around 0.65. Additionally, it is found that the TiO species also disproportionates into Ti and $TiO_{1.5}$. The calculated activity of Ti at the same temperature of 2150 K is shown in Fig. 14 in comparison with experimental data [66], where reasonable agreement is evident. Fig. 15 shows the calculated Ti–O phase diagram in the entire composition range at 1 bar total pressure. Compared to the previous assessment work [13], the associate model predicts a higher azeotropic liquid = gas equilibrium point, which is shifted to the Ti-rich side. Superimposed in this figure are gas + liquid phase equilibria data at the reduced oxygen pressure reported by Nishimura and Kimura [24],

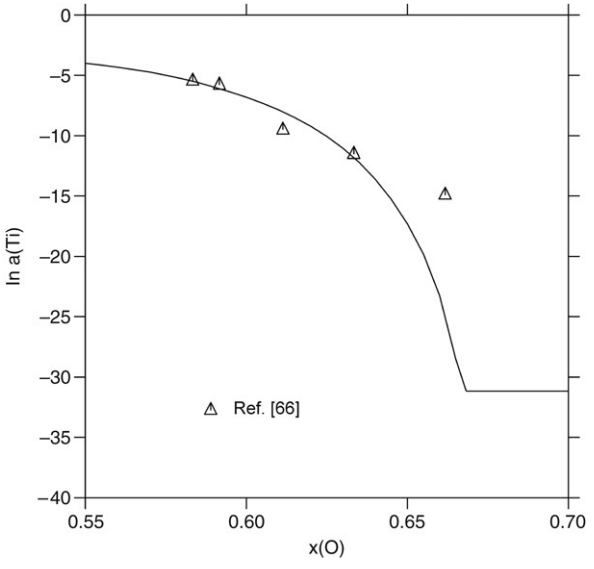

Fig. 14. Calculated activity of titanium in the liquid at 2150 K in comparison with experimental data (liquid titanium is taken as a standard state).

which are in good agreement with the calculated line for the same conditions (dash).

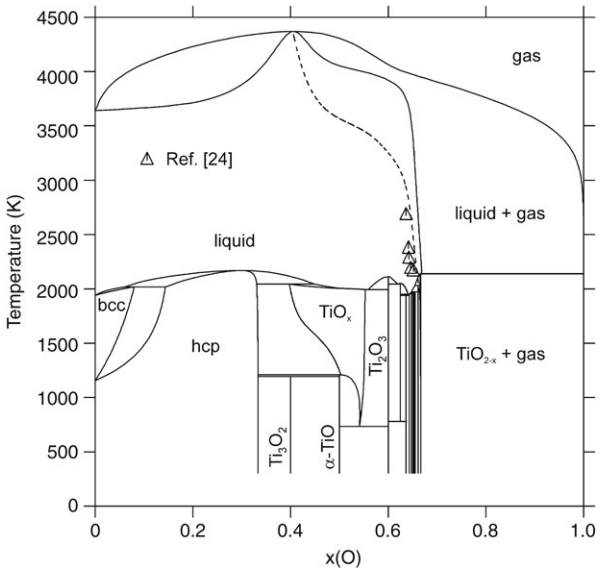

Fig. 15. Calculated Ti–O phase diagram in the entire composition range at 1 bar total pressure. The dashed line shows the oxygen isobar at $P_{O2} = 1.333 \times 10^{-4}$ bar together with the experimental data.

5. Conclusions

The associate model has been successfully employed to represent the thermodynamic properties of liquid in the Ti–O system. The Gibbs energy descriptions for most of the Magneli phases have been taken from the previous assessment work [13], while the parameters of all solution phases have been reassessed based on extensive experimental database using the compound energy formalism. A self-consistent set of the optimized Gibbs energy parameters has been derived, which allows safe extrapolations into multicomponent systems, as has been demonstrated for the Cu–Pb–Ti–Zr–O system [16].

References

[1] J.L. Murray, H.A. Wriedt, Bull. Alloy Phase Diag. 8 (2) (1987) 148–165.
[2] E.S. Bumps, H.D. Kessler, M. Hansen, Trans. ASM 45 (1953) 1008–1028.
[3] T.H. Schofield, A.E. Bacon, J. Inst. Met. 84 (1955) 47–53.
[4] P.G. Wahlbeck, P.W. Gilles, J. Am. Ceram. Soc. 49 (4) (1966) 180–183.
[5] I.I. Kornilov, Titan, The Academy of Science of USSR, Moscow, 1975.
[6] L. Kaufman, E.V. Clougherty, AIME Metall. Soc. Conf. (Proceedings), in: Metallurgy at High Pressures and High Temperatures, vol. 22, Gordon and Breach Science Publishers Inc., New York, 1964, pp. 322–380.
[7] N. Saunders, L. Chandrasekaran, J. Phase Equilibria 13 (6) (1992) 612–619.
[8] M. Pajunen, J. Kivilahti, Z. Metallkd. 83 (1) (1992) 17–20.
[9] B.J. Lee, J. Korean Inst. Met. Mater. 32 (7) (1994) 869–877.
[10] B.J. Lee, N. Saunders, Z. Metallkd. 88 (1997) 152–161.
[11] G. Eriksson, A.D. Pelton, Metall. Trans. B 24B (1993) 795–805.
[12] Y.-B. Kang, I.-H. Jung, H.-G. Lee, Calphad 30 (3) (2006) 226–234.
[13] P. Waldner, G. Eriksson, Calphad 23 (2) (1999) 189–218.
[14] W.A. Oates, H. Wenzl, Calphad 17 (1) (1993) 35–46.
[15] W.A. Oates, H. Wenzl, T. Mohri, Calphad 20 (1) (1996) 37–45.
[16] M. Cancarevic, Ph.D. Thesis, University of Stuttgart, 2007.
[17] L. Kaufman, Calphad 25 (2) (2001) 141–161.
[18] P.J. Spencer, Calphad 25 (2001) 163–174.
[19] J.O. Andersson, T. Helander, L. Höglund, P. Shi, B. Sundman, Calphad 26 (2002) 273–312.
[20] I.I. Kornilov, V.V. Glazova, Dokl. Akad. Nauk SSSR 150 (2) (1963) 313–316.
[21] R.J. Wasilewski, G.L. Kehl, J. Inst. Met. 83 (1954) 94–104.
[22] R.I. Jaffee, H.R. Ogden, D.J. Maykuth, Trans. Metall. AIME 188 (1950) 1261–1266.
[23] A.E. Jenkins, H.W. Worner, J. Inst. Met. 80 (1951) 157–166.
[24] H. Nishimura, H. Kimura, J. Jpn. Inst. Met. 20 (1956) 524–532.
[25] G. Brauer, W. Littke, J. Inorg. Nucl. Chem. 16 (1960) 67–76.
[26] A. Jostsons, P. McDougall, in: R.I. Jaffe, N.E. Promisel (Eds.), Proc. Int. Conf. Sci. Technol. Appl., Titanium, London, 1968, pp. 745–763.
[27] E. Volf, S.S. Tolkachev, I.I. Kozhina, Ser. Fiz. Khem. 2 (1959) 87–92. Vestn. Leningrad Univ., 10.
[28] E.S. Makarov, L.M. Kuznetsov, Zh. Strukt. Khim. 1 (2) (1960) 170–177.
[29] K. Suzuki, K. Sambongi, Tetsu to Hagane 58 (1972) 1579–1593.
[30] R.N. Blumenthal, D.H. Whitmore, J. Electrochem. Soc. 110 (1) (1963) 92–93.
[31] S. Zador, C.B. Alcock, High Temp. Sci. 16 (1983) 187–207.
[32] R. Tetot, C. Picard, P. Gerdanian, J. Phys. Chem. Solids 44 (11) (1983) 1059–1068.
[33] C.B. Alcock, S. Zador, B.C.H. Steele, Proc. Br. Ceram. Soc. 8 (1967) 231–245.
[34] V.A. Reznichenko, F.V. Khalimov, in: N.V. Agreev (Ed.), Protsessy. Proizvod. Titana Ego Dvuokisi, 1973, pp. 193–197.
[35] R.G. Sommer, E.D. Cater, J. Electrochem. Soc. 122 (10) (1975) 1391–1396.
[36] G. Chattopadhyay, H. Kleykamp, Z. Metallkd. 74 (3) (1983) 182–187.
[37] I.A. Vasileva, Ya.I. Gerasimov, L.P. Ogorodova, Dokl. Akad. Nauk SSSR 232 (4) (1977) 600–602.
[38] I.A. Vasileva, Ya.I. Gerasimov, E.Yu. Kushnir, Dokl. Akad. Nauk SSSR 235 (4) (1977) 839–842.
[39] A. Kozlovska-Rog, G. Rog, Pol. J. Chem. 52 (1978) 607–611.
[40] R.T. Dirstine, C.J. Rosa, Z. Metallkd. 70 (1979) 322–329.
[41] K.T. Jacob, S.M. Hoque, Y. Waseda, Mater. Trans., JIM 41 (6) (2000) 681–689.
[42] C. Picard, P. Gardanian, J. Solid State Chem. 14 (1975) 66–77.
[43] G. Boureau, P. Gerdanian, Acta Metall. 24 (1976) 717–723.
[44] R. Tetot, C. Picard, G. Boureau, P. Gerdanian, J. Chem. Phys. 69 (1) (1978) 326–331.
[45] S.M. Ariya, M.P. Morozova, E. Volf, Russ. J. Inorg. Chem. 2 (1957) 16–30.
[46] A.D. Mah, K.K. Kelley, N.L. Gellert, E.G. King, C.J. O'Brien, Thermodynamics properties of titanium–oxygen solutions and compounds, Bur. Mines Rep. Invest., Report No. 5316, 1957.
[47] O. Kubaschewski, W.A. Dench, J. Inst. Met. 82 (1953) 87–91.
[48] T.H. Okabe, R.O. Suzuki, T. Oishi, K. Ono, Mat. Trans. JIM 32 (5) (1991) 485–488.
[49] N. Sano, F. Tsukihashi, Report No. 1, 69th Committee JPSP, 1989, p. 31.
[50] S. Miyazaki, T. Oishi, K. Ono, in: G. Lutjering, U. Zwicker, W. Bunk (Eds.), Proc. 5th Int. Conf., Titanium, Munich, 1984, pp. 2657–2663.
[51] K.L. Komarek, M. Silver, Thermodynamics of nuclear material (Proc. Symp. Vienna, 1962), IAEA, Vienna, 1962, pp. 749–774.
[52] P. Kofstad, J. Phys. Chem. Solids 23 (1962) 1579–1586.
[53] K.S. Forland, Acta Chem. Scand. 18 (1964) 1267–1275.
[54] M.T. Hepworth, R. Schuhmann, Trans. Metal. Soc. AIME 224 (1962) 928–935.
[55] J.F. Marucco, B. Poumellec, J. Gautron, P. Lemasson, J. Phys. Chem. Solids 46 (1985) 709–717.
[56] J.M. Juneja, Y.J. Bhatt, S.P. Garg, J. Less-Common Metals 69 (1980) 313–318.
[57] J.F. Baumard, D. Panis, A.M. Anthony, J. Solid State Chem. 20 (1977) 43–51.
[58] J.B. Moser, R.N. Blumenthal, D.H. Whitmore, J. Am. Ceram. Soc. 48 (1965) 384.
[59] J.S. Anderson, A.S. Khan, J. Less-Common Metals 22 (1970) 219–223.
[60] R. Roy, W.B. White, J. Cryst. Growth 13–14 (1972) 78–83.
[61] R.R. Merritt, B.G. Hyde, et al., Phil. Trans. R. Soc. A 274 (1973) 627–661.
[62] W.O. Groves, M. Hoch, H.L. Johnston, J. Phys. Chem. 59 (1955) 127–131.

[63] H.Y. Wu, P.G. Wahlbeck, J. Chem. Phys. 56 (9) (1972) 4534–4540.
[64] R.I. Sheldon, P.W. Gilles, J. Chem. Phys. 66 (8) (1977) 3705–3711.
[65] S.A. Heideman, T.B. Reed, P.W. Gilles, High Temp. Sci. 13 (1980) 79–90.
[66] S. Banon, C. Chatillon, M. Allibert, High Temp. Sci. 15 (1982) 105–128.
[67] B. Granier, C. Chatillon, M. Allibert, High Temp. Sci. 23 (1987) 115–145.
[68] The SGTE unary database, version 4.4, SGTE (Scientific Group Thermodata Europe), Grenoble, France, 2001.
[69] The SGTE substance database, version 1997, SGTE (Scientific Group Thermodata Europe), Grenoble, France, 1997.
[70] M. Hillert, J. Alloys Compounds 320 (2) (2001) 161–176.
[71] R.B. McLellan, Acta Metall. 25 (11) (1977) 1241–1246.
[72] O. Redlich, A.T. Kister, Ind. Eng. Chem. 40 (2) (1948) 345–348.
[73] F. Sommer, Z. Metallkd. 73 (2) (1982) 72–76.
[74] F. Sommer, J. Non-Crys. Solids. 117–118 (1990) 505–512.
[75] S. Lele, G.V.S. Sastry, P. Ramanchandrarao, Z. Metallkd. 75 (6) (1984) 446–448.
[76] B. Predel, G. Oehme, Z. Metallkd. 65 (8) (1974) 525–530.
[77] R.C. Sharma, Y.A. Chang, Met. Trans. B 10B (1979) 103–108.
[78] B. Bjorkman, Calphad 9 (1985) 271–282.
[79] I. Obinata, Y. Takeuchi, S. Saikawa, Trans. ASM 52 (1960) 1072–1081.
[80] S. Yamaguchi, J. Phys. Soc. Jpn. 27 (1) (1969) 155–163.
[81] S. Andersson, B. Collen, U. Kuylenstierna, A. Magneli, Acta Chem. Scand. 11 (1957) 1641–1652.
[82] B. Holmberg, Acta Chem. Scand. 16 (1962) 1245–1250.
[83] A. Jostsons, A.S. Malin, Acta Crystallogr. B 24 (1968) 211–213.
[84] S. Yamaguchi, M. Koiwa, M. Hirabayashi, J. Phys. Soc. Jpn. 21 (10) (1966) 2096.
[85] I.I. Kornilov, V.V. Glazova, Zh. Neorg. Chem. 10 (7) (1965) 1660–1662. TR: Russ. J. Inorg. Chem. 10 (7) (1965) 905–907.
[86] I.I. Kornilov, V.V. Vavilova, L.E. Fykin, R.P. Ozerov, S.P. Solowiev, V.P. Smirnov, Metall. Trans. 1 (1970) 2569–2571.
[87] I.I. Kornilov, Dokl. Akad. Nauk SSSR 208 (1–3) (1973) 356–359.
[88] R.J. Wasilewski, Trans. Metall. AIME 224 (1962) 8–12.
[89] M. Koiwa, M. Hirabayashi, J. Phys. Soc. Jpn. 27 (4) (1969) 801–806.
[90] M. Hirabayashi, M. Koiwa, S. Yamaguchi, Mechanism of Phase Transformations in Crystalline Solids, Inst. Met., London, 1969.
[91] M.S. Model, G.Y. Shubina, Izv. Akad. Nauk SSSR 6 (1968) 143–157. TR: Russ. Met. 6 (1968) 97–108.
[92] A. Dubertret, P. Lehr, C. R. Acad. Hebd. Seances Sci. 263 (1966) 591–594.
[93] V.R. Porter, Ph.D. Thesis, Pennsylvania State University, 1965.
[94] I. Koncz, M. Koncz-Deri, Period. Polytech. 1 (1957) 67–87.
[95] U. Kuylenstierna, A. Magneli, Acta Chem. Scand. 10 (7) (1956) 1195–1196.
[96] S.M. Ariya, N.I. Bogdanova, Sov. Phys. Solid State 1 (7) (1960) 936–939.
[97] M.W. Chase Jr., J. Phys. Chem. Ref. Data, Monograph (9) (1998).
[98] N.P. Slyusar, A.D. Krivorotenko, E.N. Fomichev, A.A. Kalashnik, V.P. Bondarenko, High Temp. 11 (1) (1973) 190–192.